Biomedical Signal Processing and Control 39 (2018) 294–302

Contents lists available at ScienceDirect

Biomedical Signal Processing and Control

journal homepage: www.elsevier.com/locate/bspc

Research paper

Edge detection in medical images with quasi high-pass filter based on local statistics

Wei-Chun Lin [a], Jing-Wein Wang [b,*]

[a] Department of Orthopedic Surgery, Kaohsiung Municipal Min-Sheng Hospital, Kaohsiung 802, Taiwan, ROC
[b] Institute of Photonics and Communications, National Kaohsiung University of Applied Sciences, Kaohsiung 807, Taiwan, ROC

ARTICLE INFO

Article history:
Received 6 December 2016
Received in revised form 7 July 2017
Accepted 1 August 2017
Available online 30 August 2017

Keywords:
Edge detection
Medical images
WL operator

ABSTRACT

We developed a robust, quasi high-pass filter for edge detection in medical images. The kernel-based algorithm of our detector was similar to that of conventional edge detectors. The proposed edge detector has a mathematical form of local variance and is adaptive in nature. The mathematical formulation of the detector was exploited and re-expressed as a quadratic form of the Toeplitz matrix. The detector has a highly structured internal architecture with abundant spatial isotropic symmetricity. The proposed operator can greatly reduce problems frequently encountered in edge detection including fragmentation, position dislocation, and thinness loss. The detector is robust to noise and can efficiently extract crucial edge features. We named this new operator as the WL operator (Wang and Lin). The performance of the WL operator was compared to that of other edge detectors by using Pratt's figure of merits. In addition, the performance was confirmed with experts by using visual analog scale scores. The results obtained using the WL operator for different medical imaging modalities including X-ray, CT, and MRI are promising. Therefore, the WL operator warrants further investigation.

1. Introduction

Edge detection is a challenging task often encountered in image processing. Edge detection plays a crucial role in image segmentation and other preprocessing fields [1]. The success of subsequent high-level processing highly depends on these preprocessing tasks [2]. However, edge detection is often difficult in medical images such as X-rays, CT, and MRI. Medical images are often blurred because of intrinsic physical processes required for acquiring them. The management of blurred images by using traditional edge detection operators is difficult because of the Mach effect. Human eyes can identify most subtle parts of object boundaries even in the presence of blurring. In the case of a slowly changing blurred margin, the human vision often outperforms the computer vision. However, extraction of the correct margin in a severely blurred image is challenging [3]. The separation of a scene into an object and a background is an essential step in image interpretation. This process is effortlessly performed by the human visual system. However, when computer vision algorithms are designed to mimic this action, several problems can be encountered. Because of the presence of noise in an image, location of edge maps in the absence of real edges is possible. For similar reasons, it is also possible to completely miss existing edges. The degree of success of an edge detector depends on its ability to accurately locate true edges [4]. When interpreting medical images, human eyes can discern the blurred margin of most objects by adjusting detection scales effortlessly. By contrast, the scale adjustment always requires extra attention in the machine vision [5]. Moreover, human visual systems are robust to minor illumination and positional changes. However, combating the positional and illumination variation on the machine vision is of great concern [6].

Conventional edge detectors are usually sensitive to noise because of their high-frequency amplification property [7]. However, real medical images have high readout and photon noises. Traditional edge detectors are intrinsically high-pass filters; therefore, their noise power spectrum always tends to be exaggerated in the detection process. Accurate extraction of high-frequency components of image structures such as edges without amplification of undesired noise is crucial for the design of an edge detector [8]. Directional propensity is another disadvantage of the conventional kernel-based operator. Directional invariance should be the basic requirement of a robust edge detector [9]. In practice, this always requires manual adjustment by the performers themselves. Various solutions such as combining the horizontal and vertical Sobel's operator can be applied. However, different combination weights

* Corresponding author at: Graduate Institute of Photonics and Communications, National Kaohsiung University of Applied Sciences, No. 415, Jiangong Rd., Sanmin District, Kaohsiung City 80778, Taiwan, ROC.
E-mail addresses: jwwang@kuas.edu.tw, jwwang_2005@yahoo.com.tw (J.-W. Wang).

http://dx.doi.org/10.1016/j.bspc.2017.08.011
1746-8094/

remain to be justified in this circumstance. As a result, many parameters in conventional kernel methods are quite arbitrary and not parsimonious in implementation. Thus, solving this issue of artificial parameter design is necessary [10]. In this paper, we proposed a new edge detection model that is free of arbitrary parameters. The proposed model can accurately locate the edge and is robust to noise. The characteristics of our proposed detector are discussed in the following sections.

The remaining paper is organized as follows. Some of the existing methods are described in Section 2, and the proposed method is described in Section 3. Some experiments based on our method are presented in Section 4, and the paper is concluded in Section 5.

2. Edge detection operators

2.1. Previous work

Over the years, many methods have been proposed for detecting edges in images. Some of the earlier methods, such as Sobel's and Prewitt's detectors, used local gradient operators that detected only edges having specific orientations and performed poorly when the edges were blurred and noisy [11,12]. Combining such directional operators to approximate the performance of a rotationally invariant operator is possible. Various algorithms that are immune to noise, non-directional, and can detect a more accurate location of the edge have been developed. A majority of these algorithms are linear operators that are derivatives of some types of smoothing filters. Torre and Poggio [13] suggested that edge detection is a problem in numerical differentiation and demonstrated that numerical differentiation of images is an ill-posed problem. Differentiation amplifies high-frequency components, thus exaggerating noise in the image data. However, differentiation is a mildly ill-posed problem that can be transformed into a well-posed problem by using several methods. Marr and Hildreth [14] proposed convolving the signal by using a rotationally symmetric Laplacian of Gaussian (LoG) mask and by locating zero crossings of the resulting output where the amount of smoothing is controlled by the variance of the Gaussian. The Gaussian filter is thus far the most widely used smoothing filter in edge detection [15]. This method is theoretically favorable because the localization properties of the Gaussian filter in both spatial and frequency domains makes it an optimal filter for edge detection [16]. Although the Gaussian filter reduces noise, it affects genuine and essential high-frequency edge features, and reduces edge localization accuracy in low-contrast images. Other methods such as multi-scale techniques can be used to address this problem [17]. However, selection of the appropriate step between scales and combining corresponding edge contours remains a major problem [18]. The edge location accuracy of the Canny edge detector is higher than that of the LoG-based approach, and the local extreme of the Canny edge detector's output may have desirable behaviors in the scale space [19]. However, the Canny detector is complex and time consuming, and there remains parameters to be determined in order to obtain optimal results [20].

2.2. The proposed edge detector

The WL operator was defined within a 3×3 neighborhood around a single center pixel $I(x, y)$ in I, where $I(x, y)$ is the input image of the size $W \times H$. The local intensity mean μ_I and local signal energy variation ε of the 3×3 neighborhood pixels were defined using the following expressions:

$$\mu_I(x, y) = \frac{1}{N} \sum_{i=-1}^{1} \sum_{j=-1}^{1} I(x+i, y+j) \tag{1}$$

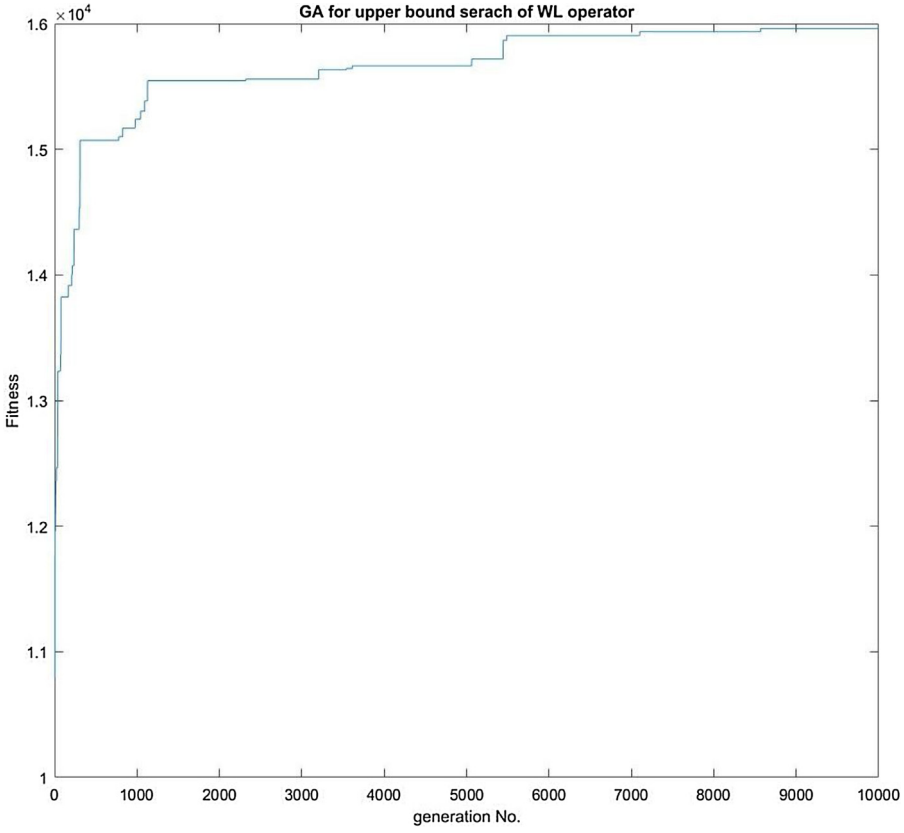

Fig. 1. Genetic algorithm evaluation for upper bound value of the WL operator.

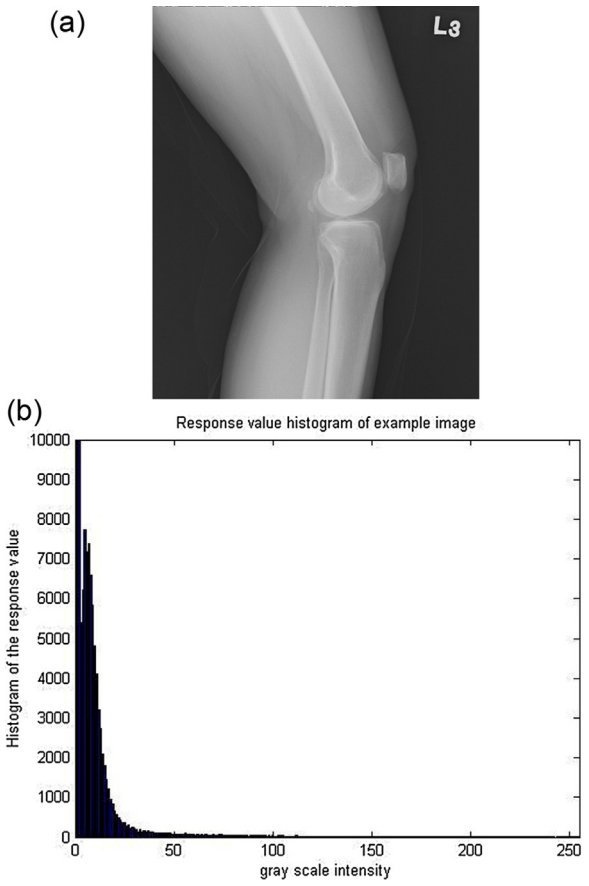

Fig. 2. (a) Lateral view of the human knee X-ray. (b) Response value histogram of the WL operator.

$$\varepsilon(x,y) = \frac{1}{N}\sum_{i=-1}^{1}\sum_{j=-1}^{1}(I(x+i,y+j) - \mu_I(x,y))^2 \tag{2}$$

where $N=9$ is a normalizing constant. For transforming the gray-scale intensity images into logical maps, we proposed a thresholding procedure as follows: the global mean depending on $\varepsilon(x,y)$ is defined as

$$\mu_g = \frac{1}{W\times H}\sum_{x=0}^{W-1}\sum_{y=0}^{H-1}\varepsilon(x,y) \tag{3}$$

A thresholded image is produced as

$$B(x,y) = Thresholding\ of\ I(x,y) = \begin{cases} 1, & if\ \varepsilon(x,y) \geq \mu_g \\ 0, & otherwise \end{cases} \tag{4}$$

In general, there are 2 choices for the application of the WL operator in edge extraction. If a binary logical map is intended, then the thresholding procedure with a global parameter would be performed, as described. Otherwise, we suggest that the thresholding procedure will not be performed. Because the response value obtained by the WL operator is greater than or equal to zero, setting the response value large than 255 to this ceiling will generate an intensity map. The motivation of this scheme is its inherent capacity to present the degree between "strong" and "weak" edge structures by using the 8-bit coding in a gray-scale image format. Once the binary logical map was obtained using the thresholding procedure, some information was deemed to be lost during the transformation. In practice, we observed that the non-thresholded version was more similar to the scene discerned by the human eyes because it contains more information than the thresholded version does.

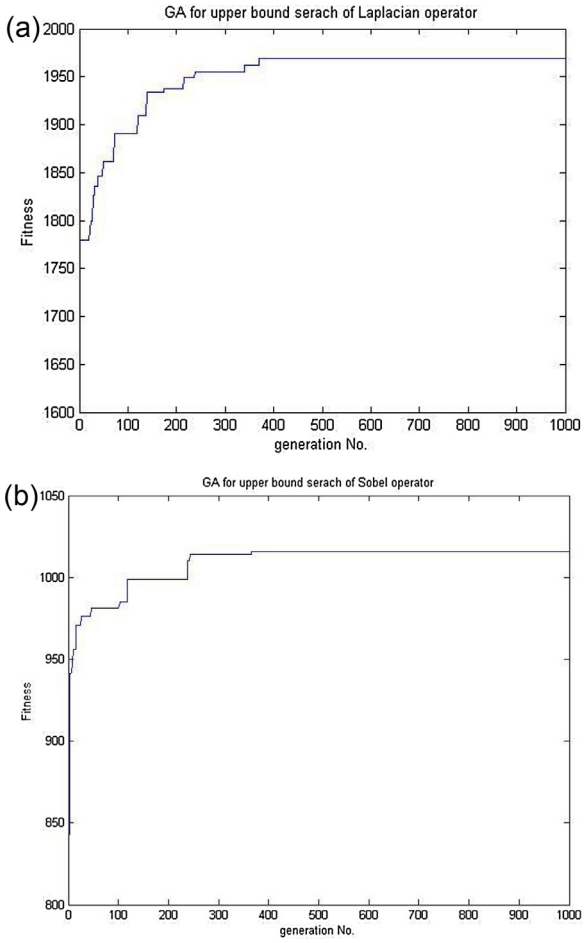

Fig. 3. (a) Genetic algorithm for the upper bound search of the Laplacian operator. (b) Genetic algorithm for the upper bound search of Sobel's operator.

3. Properties of the WL operator

3.1. Quadratic form presentation of the WL operator

The WL operator is very similar to the mathematical form of mean and variance in statistics. Some intriguing correspondence is present between the variance form and kernel-based high-pass filters. Considering the 3×3 neighborhood elements of the kernel operator as a column vector, it can be described as $\boldsymbol{x} = [x_1, x_2, x_3, \cdots x_9]^t$. The Eq. (2) can then be rewritten in a quadratic form:

$$\varepsilon(x,y) = \frac{1}{N^2}\boldsymbol{x}^t\boldsymbol{C}\boldsymbol{x} \tag{5}$$

$$\text{where } \boldsymbol{C} = \begin{bmatrix} 8 & -1 & -1 & -1 & -1 & -1 & -1 & -1 & -1 \\ -1 & 8 & -1 & -1 & -1 & -1 & -1 & -1 & -1 \\ -1 & -1 & 8 & -1 & -1 & -1 & -1 & -1 & -1 \\ -1 & -1 & -1 & 8 & -1 & -1 & -1 & -1 & -1 \\ -1 & -1 & -1 & -1 & 8 & -1 & -1 & -1 & -1 \\ -1 & -1 & -1 & -1 & -1 & 8 & -1 & -1 & -1 \\ -1 & -1 & -1 & -1 & -1 & -1 & 8 & -1 & -1 \\ -1 & -1 & -1 & -1 & -1 & -1 & -1 & 8 & -1 \\ -1 & -1 & -1 & -1 & -1 & -1 & -1 & -1 & 8 \end{bmatrix} \tag{6}$$

with the normalizing constant $N=9$, and the matrix $\boldsymbol{C}$ in the center of the quadratic form has some appealing properties. It is a Toeplitz matrix with a main diagonal component of $N-1$ with all other elements equaling to -1. This formulation can facilitate the calculation

Fig. 4. (a) Edge detection performed on the human knee X-ray by using the WL operator. (b) Edge detection performed on the human knee X-ray by using Sobel's operator. (c) Edge detection performed on the human knee X-ray by using the Canny operator. (d) Edge detection performed on the human knee X-ray by using the LoG method.

of the desired response value without a rounding error during the subtraction operation by using Eq. (2).

By combining the first 2 terms in the right hand side of Eq. (5), we obtained a matrix operator $\boldsymbol{D}$ with its transpose $\boldsymbol{D}^{\boldsymbol{t}}$ as the following form:

$$\boldsymbol{D}^{\boldsymbol{t}} = \begin{bmatrix} +8x_1 - x_2 - x_3 - x_4 - x_5 - x_6 - x_7 - x_8 - x_9 \\ -x_1 + 8x_2 - x_3 - x_4 - x_5 - x_6 - x_7 - x_8 - x_9 \\ -x_1 - x_2 + 8x_3 - x_4 - x_5 - x_6 - x_7 - x_8 - x_9 \\ -x_1 - x_2 - x_3 + 8x_4 - x_5 - x_6 - x_7 - x_8 - x_9 \\ -x_1 - x_2 - x_3 - x_4 + 8x_5 - x_6 - x_7 - x_8 - x_9 \\ -x_1 - x_2 - x_3 - x_4 - x_5 + 8x_6 - x_7 - x_8 - x_9 \\ -x_1 - x_2 - x_3 - x_4 - x_5 - x_6 + 8x_7 - x_8 - x_9 \\ -x_1 - x_2 - x_3 - x_4 - x_5 - x_6 - x_7 + 8x_8 - x_9 \\ -x_1 - x_2 - x_3 - x_4 - x_5 - x_6 - x_7 - x_8 + 8x_9 \end{bmatrix} \quad (7)$$

The operator $\boldsymbol{D}$ had circular symmetricity in its components. However, the matrix $\boldsymbol{D}$ differed from the matrix $\boldsymbol{C}$ in that it contained parameters from neighborhood image pixels. This indicates that the WL operator is an adaptive filter. In contrast to conventional filters with constant kernel elements, the WL operator has different kernel elements on different positions of the image. Moreover, compared with other high-pass filters, the WL operator achieves quasi high-pass filter property as the coefficient sum of the matrix $\boldsymbol{D}$ becomes zero. The high-pass property depicted in Eq. (7) renders the WL operator the ability of edge enhancement.

3.2. Isotropic symmetricity of the WL operator

The WL operator has abundant directional symmetricities. With some algebraic manipulation, the Eq. (2) can be expressed as:

$$\varepsilon(x,y) = \frac{1}{N^2}\left[(x_1 - x_2)^2 + (x_1 - x_3)^2 + (x_1 - x_4)^2 + \cdots + (x_8 - x_9)^2\right] \quad (8)$$

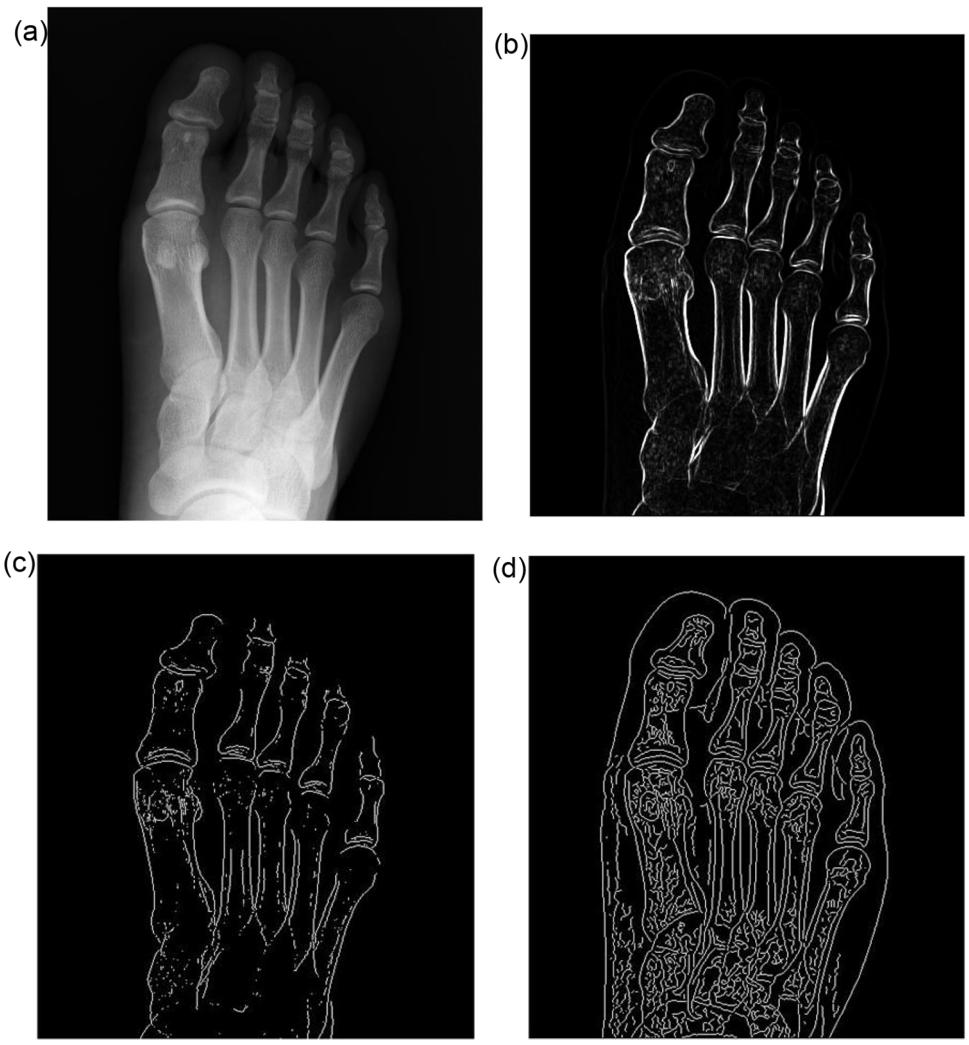

Fig. 5. (a) Anterior–posterior view of the human foot X-ray. (b) Edge detection performed on the human foot X-ray by using the WL operator. (c) Edge detection performed on the human foot X-ray by using Sobel's operator. (d) Edge detection performed on the human foot X-ray by using the Canny operator.

With permutation of square terms in the 3×3 kernel pixel values in Eq. (8), there exists C_2^9 of total 36 directive components in the response value, and this is higher than that in other constant value operators. Isotropic symmetricity is the most appealing property of our WL operator. Thus, it has less directional propensity and can outperform other edge detectors in this aspect.

3.3. Dynamic range of the WL operator

The response value overflow is common in the practice of edge detection. In contrast to a smoothing low-pass filter, the response value of most high-pass filters often has a higher dynamic range than the original intensity matrix. From Eq. (2), it is evident that the lower bound of $\varepsilon(x, y)$ is zero. However, the upper bound remains to be evaluated. The upper bound of the$\varepsilon(x, y)$ depends on 9 input values ranging from 0 to 255. Solving this extremity value problem by using traditional techniques such as system of linear equations is difficult. We used the genetic algorithm approach for evaluation of the upper bound value. We performed genetic algorithms by using following parameters: population size = 2000, bit number = 8, variable number = 9, range = 0–255, crossover rate = 0.7, mutation rate = 0.1, and generation number = 10,000. The genetic algorithm was performed using the implemented elitism strategy. The fitness function was chosen as the response value of the WL operator. The fitness function with the generation number is presented in Fig. 1. The dynamic range of the WL operator is approximately from zero to 1.6×10^4. The value can be close to the upper bound if the input vector is similar to the solution vector found by the genetic algorithm. Otherwise, the response value cannot be close to the upper bound because the extremely large response value is seldom noted owing to the nature of image pixel values.

3.4. Histogram of the WL operator response in medical images

The dynamic range of the WL operator response value is higher than that of the ordinary gray-scale image of 0–255. The lower bound of the WL operator coincides with that of the gray-scale intensity image; however, the upper bound encounters the problem of overflow. We can treat the overflow portion by mapping on the ceiling value. By contrast, the response value of the WL operator is totally dependent on the input vector of 3×3 neighborhood. For example, the X-ray film of the lateral view of the human knee is presented in Fig. 2(a). The response value histogram of the WL operator in this sample image is illustrated in Fig. 2(b). The overflow portion of the histogram in Fig. 2(b) was 0.029% with a maximum intensity value of 756 in this case. The maximum value generated from this image is much lower than the obtained upper bound value. At the same time, the overflow portion is less, indicating that the remapping procedure will not highly distort the image information.

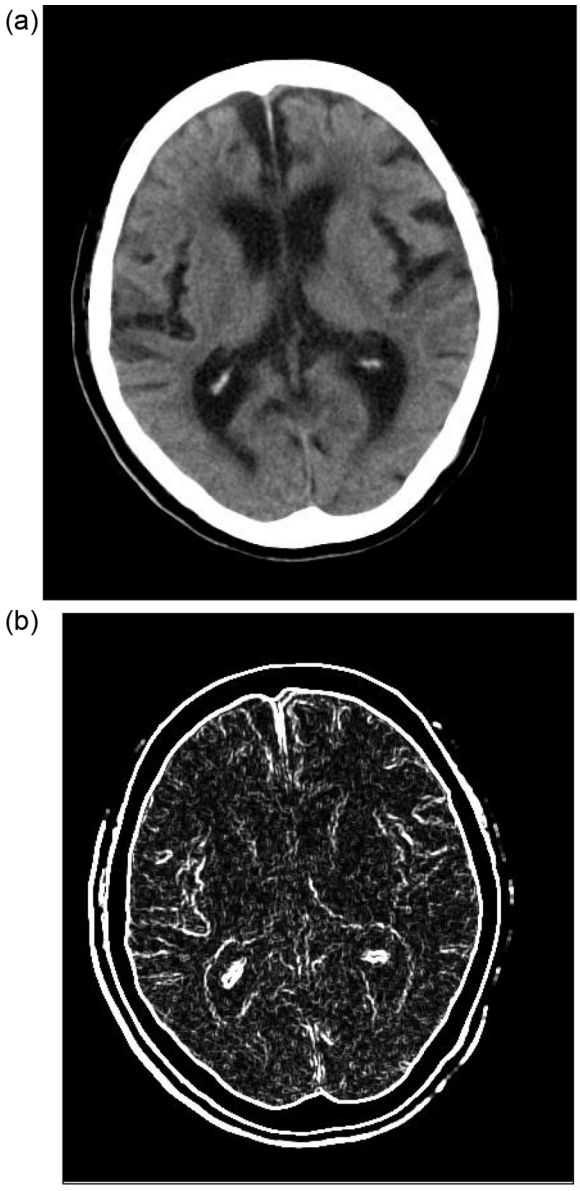

Fig. 6. (a) Human brain CT. (b) Edge detection performed on the human brain CT by using the WL operator.

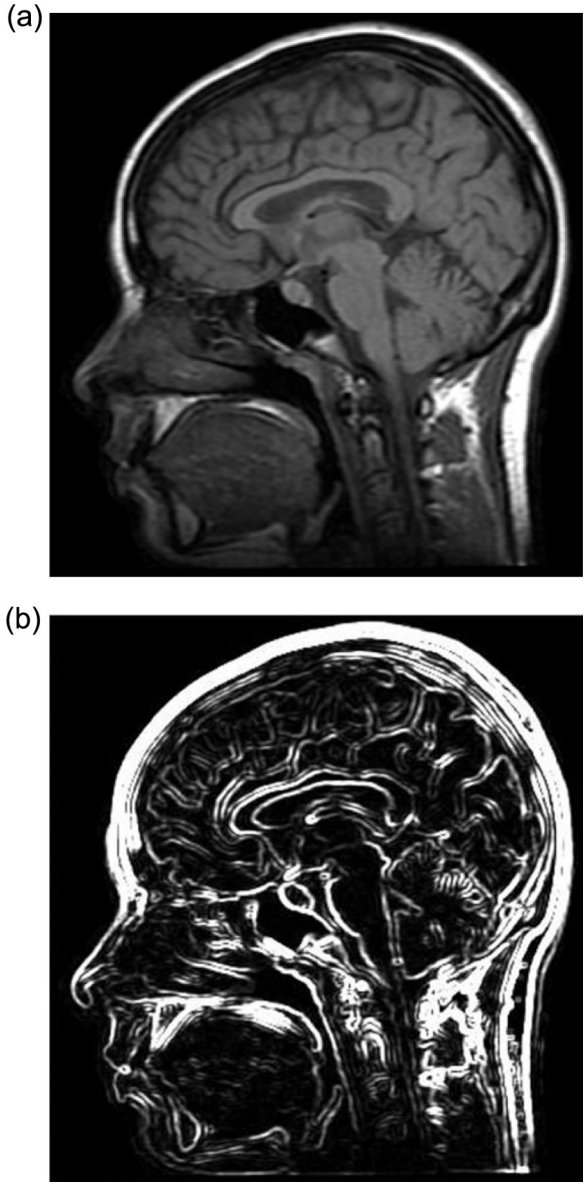

Fig. 7. (a) Human brain MRI, sagittal view. (b) Edge detection performed on the human brain MRI by using the WL operator.

3.5. Correspondence with other edge detectors

The proposed WL operator is adaptive in nature. Its action depends on the input vector on the 3×3 neighborhood of the local intensity image. In some circumstances, the WL operator corresponds to the Laplacian or Sobel's operator if the input vector matches some specific configurations. The frequency responses of Laplacian and Sobel's operators can be regarded as specific subsets of the WL operator. The Laplacian operator on 3×3 neighborhood is expressed as:

$$Laplacian = \begin{bmatrix} -1 & -1 & -1 \\ -1 & 8 & -1 \\ -1 & -1 & -1 \end{bmatrix} \tag{8}$$

The Sobel's operation is expressed as:

$$Sobel = \begin{bmatrix} -1 & 0 & 1 \\ -2 & 0 & 2 \\ -1 & 0 & 1 \end{bmatrix} \tag{9}$$

Because the high-pass filter requires that the matrix coefficient should equal to zero, the response value overflow may be encountered in both negative and positive directions. We could define the response value of these 2 operators as absolute values after calculating the 3×3 neighborhood of image pixels such that the lower bound value of both operators is zero. However, the upper bound value of these 2 operators should be evaluated numerically. In addition, we formulated this upper bound problem as an optimization process to be tackled through the genetic algorithm technique. The convergence curves are presented in Fig. 3(a) and (b) for Laplacian and Sobel's operators, respectively. Conjecturing the upper bound value of the response of Laplacian and Sobel's operators directly and the values corresponding to the searched results perfectly is feasible. The upper bounds are all within the dynamic range of the WL operator. For every response value from the kernel operator, many input vector configurations are present on 3×3 neighborhood of local images. Therefore, the response value range of Laplacian and Sobel's operators can be regarded as a subset of the WL operator.

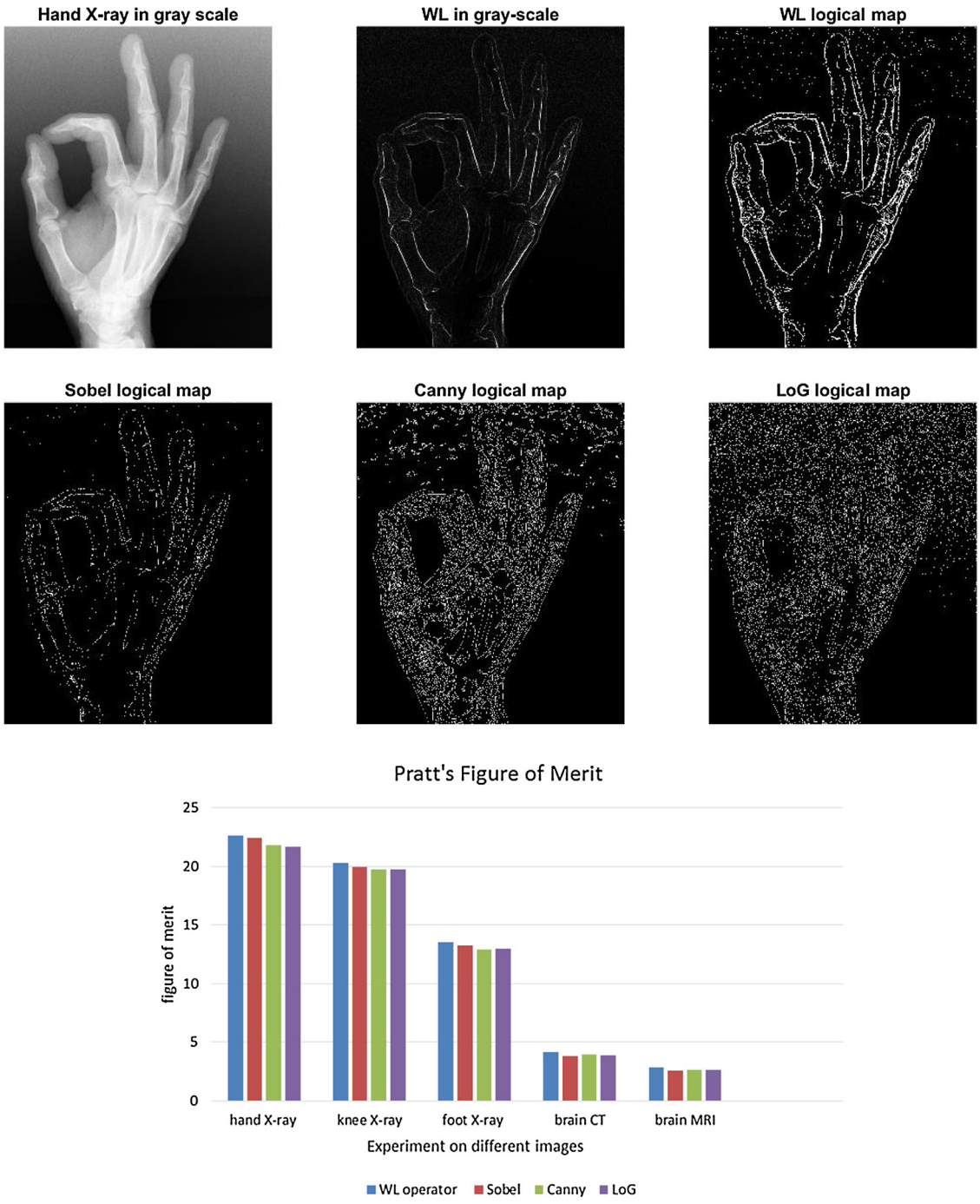

Fig. 8. (a) Edge logical map from hand X-ray image using different edge detectors. (b) Pratt's figure of merits plot of 5 different images.

4. Experimental results and discussion

We performed several experiments to demonstrate the performance of the WL operator. Because of space limitation, we have included a subset of the results. We selected approximately 512×512 as the tested picture size to reduce the variation in the image scale. In the first experiment, we used the lateral view of the human knee presented in Fig. 2(a) as the input image. In addition, we compared 3 common edge detectors, namely Sobel's, Canny, and LoG-based detectors, with the WL operator. As presented in Fig. 4(a), the edge obtained using the WL operator was thin, continuous, and well-localized. Moreover, the WL operator detected most of the vital object contours. As presented in Fig. 4(b), the edge obtained using Sobel's operator was severely fragmented and lost almost all the vertical components. This issue can be solved by adding another vertical-oriented Sobel's operator and by superimposing the 2 images to compensate the directional propensity. The relative weight between vertical and horizontal components should be adjusted to obtain optimal results. This problem is frequently encountered when applying Sobel's operator. Thus, Sobel's operator cannot perform uniformly, particularly in medical images. By contrast, the WL operator can provide a united frame without artificial parameter adjustment. As presented in Fig. 4(c), the directional propensity of the edge obtained using the Canny detector was lower than that of the edge obtained using Sobel's operator. In addition, line fragmentation of the edge obtained using the Canny

Table 1
(a) Visual analog scale score statistics with ANOVA.

Descriptives							
VAS score							
	N	Mean	Std. Deviation	Std. Error	95% Confidence Interval for Mean		Minimum	Maximum
					Lower Bound	Upper Bound		
WL operartor	10	8.3000	1.31656	0.41633	7.3582	9.2418	6.00	10.00
Sobel	10	2.5000	0.81650	0.25820	1.9159	3.0841	1.00	3.50
Canny	10	3.7000	1.03494	0.32728	2.9596	4.4404	2.40	5.60
LoG	10	4.0700	1.55781	0.49262	2.9556	5.1844	2.10	6.70
Total	40	4.6425	2.50598	0.39623	3.8410	5.4440	1.00	10.00

(b) Significance report of the visual analog score statistics with ANOVA.

ANOVA					
VAS score					
	Sum of Squares	df	Mean Square	F	Sig.
Between Groups	191.837	3	63.946	43.368	0.000
Within Groups	53.081	36	1.474		
Total	244.918	39			

(c) Post Hoc comparison of visual analog score statistics.

Multiple Comparisons						
VAS score						
Scheffe						
(I) Treatment Methods	(J) Treatment Methods	Mean Difference (I-J)	Std. Error	Sig.	95% Confidence Interval	
					Lower Bound	Upper Bound
WL opeartor	Sobel	5.80000*	0.54304	0.000	4.2076	7.3924
	Canny	4.60000*	0.54304	0.000	3.0076	6.1924
	LoG	4.23000*	0.54304	0.000	2.6376	5.8224
Sobel	WL opeartor	−5.80000*	0.54304	0.000	−7.3924	−4.2076
	Canny	−1.20000	0.54304	0.200	−2.7924	0.3924
	LoG	−1.57000	0.54304	0.055	−3.1624	0.0224
Canny	WL opeartor	−4.60000*	0.54304	0.000	−6.1924	−3.0076
	Sobel	1.20000	0.54304	0.200	−0.3924	2.7924
	LoG	−0.37000	0.54304	0.926	−1.9624	1.2224
LoG	WL opeartor	−4.23000*	0.54304	0.000	−5.8224	−2.6376
	Sobel	1.57000	0.54304	0.055	−0.0224	3.1624
	Canny	0.37000	0.54304	0.926	−1.2224	1.9624

* The mean difference was significant at the 0.05 level.

detector was lower than that of the edge obtained using Sobel's operator. However, the Canny detector was vulnerable to noise amplification and spurious edges. We observed that almost all the striation in bone and muscle tissues were detected and amplified as distinct edges. Because readout and photon noises are very common in medical images, the Canny detector should be applied in medical images with caution. Compared with Fig. 4(c), Fig. 4(a) is more efficient in noise suppression and still can exhibit striation details within the bone and muscle tissues with evident gross object boundaries. The results obtained using the LoG method are presented in Fig. 4(d). The LoG operator is conceptually similar to the Canny detector; however, the LoG operator has a low-pass filter component. The application of the LoG operator in human X-rays remains unsatisfactory.

An X-ray of the human foot is presented in Fig. 5(a). The WL operator was applied and the results are illustrated in Fig. 5(b). The results of Sobel's and Canny detectors are presented in Fig. 5(c) and (d). The bony contour is correctly depicted in Fig. 5(b) without loss of small bones, and the bone marrow texture is presented in a satisfactory way without many spurious edges. We also used the WL operator in human brain CT images, as illustrated in Fig. 6(a) and (b). The WL operator efficiently detected edges even in the brain parenchyma area. As presented in Fig. 6(b), brain parenchyma architectures such as the sulcus and ventricles were well demarcated with accurate localization. A human brain MRI in the sagittal view is presented in Fig. 7(a). The WL operator was applied and its results are presented in Fig. 7(b). The central nervous system was demarcated with accurate extraction of the precise boundaries and contours of the thalamus, pons, and cerebellum.

To objectively validate the performance of the WL operator, we used the criteria proposed by Pratt [21]. Pratt's Figure of Merit (FOM) is given as follows:

$$\text{Figure of Merit} = \frac{1}{\max\left\{I_I | I_A\right\}} \sum_{i=1}^{I_A} \frac{1}{1 + a d_i^2} \tag{10}$$

Where I_I and I_A are the number of ideal and actual edge map points, respectively; d is the distance of an actual edge point to the ideal point; and a is the scaling constant. The separation distance d plays a vital role in the evaluation of the Pratt's FOM. From Eq. (10), it could be observed that the FOM is inversely proportional to the distance d. Obtaining an ideal edge map as a gold standard is a key issue. In this study, we asked 3 physicians to manually characterize the ideal edge map. This ideal edge map was then used for comparing maps

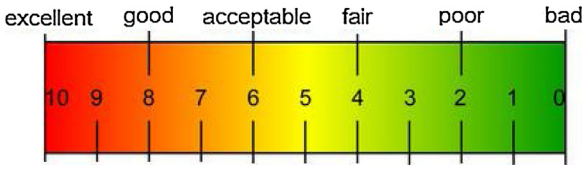

Fig. 9. Visual Analog Scale for image assessment.

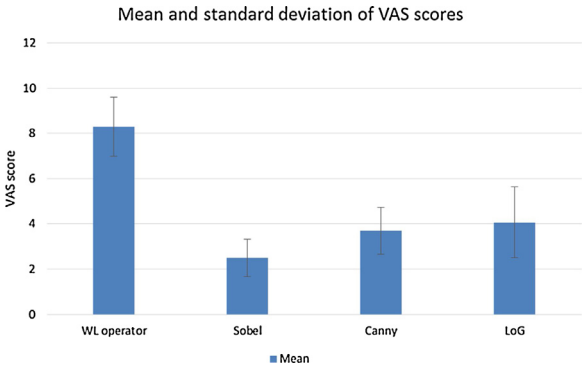

Fig. 10. Mean plot between different methods.

generated using other edge detectors. The proposed WL operator was compared with Sobel's, Canny, and LoG operators by using 5 medical images including hand X-ray, knee X-ray, foot X-ray, brain CT, and brain MRI. In Fig. 8(a), a hand X-ray image which has background noise caused by light contamination is shown. The logical map obtained by WL operator is more robust to noise compared to LoG method. For other images, as presented in Fig. 8(b), the FOM of the WL operator was higher than that of the other operators.

To further validate the WL detector, we used an alternative evaluation method. We designed a semi-quantitative visual score for comparing different images to assess the quality of obtained images. This method was developed from the clinical situation of pain assessment [22]. A visual analog scale (*VAS*) is a measurement instrument used to assess patient's pain on a semi-quantitative basis [23]. A *VAS* is presented as a horizontal line, 100 mm in length, anchored with word descriptors at each end. We designed our own VAS for image quality assessment, as illustrated in Fig. 9. The application of edge detection in medical images has major implications in subsequent high-level processing such as diagnosis, fracture identification, and lesion localization. All these tasks demand sophisticated skills of highly trained personnel such as radiologists or clinical physicians. The experts often cannot express well-documented rules when working with relevant features of medical images. Therefore, the quality of image processing should be assessed by experts directly. For this reason, we designed the VAS measurement tool. The scores of the VAS were provided by 10 independent physicians. We used the images treated using the WL operator as the contrast group and asked the physicians to evaluate the VAS scores of Sobel's, Canny, and LoG operators. The VAS scores were provided on an ordinal scale. We calculated the score difference by using analysis of variance (ANOVA), and the statistical results of SPSS are listed in Table 1a–c and Fig. 10. The null hypothesis was set as no difference between 2 treatments, and type I error (α error) was set to 0.05. As demonstrated by post hoc comparison between treatments in Table 1c, all p values were significant (<0.05). Therefore, the benefit of our proposed method was confirmed using the ANOVA test with VAS scores.

5. Conclusion

We investigated the application of the WL operator in edge detection of medical images. The proposed WL operator is similar to the mathematical form of variance and is adaptive in nature. The proposed method is efficient for edge detection in medical images. It has abundant isotropic symmetricity and quasi high-pass filtering property. The WL operator can be applied to different imaging modalities including X-ray, CT, and MRI. The WL operator is robust to noise and can efficiently extract crucial edge features contained in object boundaries. The performance of the WL operator was compared to that of other methods and evaluated using Pratt's FOM and VAS. The WL operator outperformed other methods in this study and thus warrants further evaluation.

Acknowledgment

This study was funded by the Ministry of Science and Technology, Taiwan, under project code MOST 104-2221-E-151-026.

References

[1] R.C. Gonzalez, R.E. Woods, Digital Image Processing, 3rd edition, Prentice-Hall, Englewood Cliffs, NJ, 2008.
[2] A.E.A. Elaraby, E.H.B. Mohamed, M. Heshmat, M. Hassaballach, A.S. Abdel Rady, Edge detection of noisy medical images based mixed entropy, Comput. Eng. Intell. Syst. 4 (13) (2013) 97–106.
[3] M. Basu, Gaussian-based edge-detection methods a survey, IEEE Trans. Syst. Man Cybern. 32 (3) (2002) 252–260.
[4] D. Xu, T. Kasparis, Detection and localization of edge contours, Proc. of SPIE 5097 (2003) 79–89.
[5] J. Shotton, A. Blake, R. Cipolla, Multi-scale categorical object recognition using contour fragments, IEEE Trans. Pattern Anal. Mach. Intell. 30 (7) (2008) 1270–1281.
[6] G. Papari, N. Petkov, Edge and line oriented contour detection: state of the art, Image Vis. Comput. 29 (2011) 79–103.
[7] H. Li, X. Liao, C. Li, H. Huang, C. Li, Edge detection of noisy images based on cellular neural networks, Commun. Nonlinear Sci. Numer. Simul. 16 (2011) 3746–3759.
[8] P.L. Shui, W.C. Zhang, Noise-robust edge detector combining isotropic and anisotropic Gaussian kernels, Pattern Recognit. 45 (2) (2012) 806–820.
[9] C. Lopez-Molina, M. Galar, H. Bustince, B. De Baets, On the impact of anisotropic diffusion on edge detection, Pattern Recognit. 47 (1) (2014) 270–281.
[10] Z.J. Hou, G.W. Wei, A new approach to edge detection, Pattern Recognit. 35 (2002) 1559–1570.
[11] S. Gupta, S.G. Mazumda, Sobel edge detection algorithm, Int. J. Comput. Sci. Manag. Res. 2 (2) (2013) 1578–1583.
[12] Rashmi, M. Kumar, R. Saxena, Algorithm and technique on various edge detection: a survey, Signal Image Process.: An Int. J. (SIPIJ) 4 (3) (2013) 65–75.
[13] V. Torre, T. Poggio, On edge detection, IEEE Trans. Pattern Anal. Mach. Intell. 2 (1986) 147–163.
[14] D. Marr, E. Hildreth, Theory of edge detection, Proc. R. Soc. Lond. B 207 (1980) 187–217.
[15] G.T. Shrivakshan, A comparison of various edge detection techniques used in image processing, Int. J. Comput. Sci. Issues 9 (5) (2012) 269–276.
[16] C. Lopez-Molina, B. De Baets, H. Bustince, J. Sanz, E. Barrenechea, Multiscale edge detection based on Gaussian smoothing and edge tracking, Knowl. Based Syst. 44 (2013) 101–111.
[17] W.G. Zhang, Q. Zhang, C.S. Yang, Edge detection with multiscale products for SAR image despeckling, Electron. Lett. 48 (4) (2012) 211–212.
[18] C. Lopez-Molina, B. De Baets, H. Bustince, Quantitative error measures for edge detection, Pattern Recognit. 46 (2013) 1125–1139.
[19] R. Maini, H. Aggarwal, Study and comparison of various image edge detection techniques, Int. J. Image Process. 3 (1) (2009) 1–11.
[20] P. Qiu, B. Yandell, Jump detection in regression surfaces, J. Comput. Graph. Stat. 6 (3) (1997) 332–354.
[21] S. Pande, V.S. Bhadouria, D. Ghoshal, A study on edge marking scheme of various standard edge detectors, Int. J. Comput. Appl. 44 (9) (2012) 33–37.
[22] P.S. Myles, S.T. Troedel, M. Boquest, M. Reeves, The pain visual analog scale: is it linear or nonlinear? Anesth. Analg. 89 (1999) 1517–1520.
[23] F. Dexter, D.H. Chestnut, Analysis of statistical tests to compare visual analog scale measurements among groups, Anesthesiology 82 (4) (1995) 896–902.